These data seem to be sufficient to explain the dust data in Antarctica. To explain the Greenland data (enhancement by a factor of 100), we need to account for a further factor of about 3. During the LGM, the Northern Hemisphere had more deserts (*20*) and large areas of land that were covered by ice sheets. The denudation of boreal forests and the formation of loess (*21*) could have contributed additional sources of continental dust.

It remains a challenge to atmospheric modeling to explain why the hydrologic cycle during the LGM (as revealed in the dust washout lifetime) was so greatly weakened (*22*). One interesting possibility is that the enhanced amount of dust might have played an active role in modifying the climate of the LGM (*23*). In this case, dust may be more than an indicator of climate change; dust itself could be an agent of climate change, as it is on our sister planet Mars (*24*).

REFERENCES AND NOTES

1. Intergovernmental Panel on Climate Change, *Climate Change: The IPCC Scientific Assessment* (Cambridge Univ. Press, Cambridge, 1990); *Climate Change 1992: Supplement to the IPCC Scientific Assessment* (Cambridge Univ. Press, Cambridge, 1992); C. A. Senior and J. F. B. Mitchell, *J. Climate* **6**, 393 (1993); B. C. Weare, *ibid.* **7**, 248 (1994); R. D. Cess *et al.*, *J. Geophys. Res.* **95**, 16601 (1990).
2. R. S. Lindzen, *Bull. Am. Meteor. Soc.* **71**, 288 (1990); *ibid.*, p. 1465.
3. D. Rind and D. Peteet, *Quat. Res.* **24**, 1 (1985); T. J. Crowley and G. R. North, *Paleoclimatology* (Oxford Univ. Press, Oxford, 1991); J. E. Hansen *et al.*, in *Climate Processes and Climate Sensitivity*, J. E. Hansen and T. Takahashi, Eds. (Geophysical Monograph 29, American Geophysical Union, Washington, DC, 1984), pp. 130–163.
4. J.-R. Petit *et al.*, *Nature* **293**, 391 (1981).
5. C. U. Hammer *et al.*, in *Greenland Ice Core: Geophysics, Geochemistry, and the Environment*, C. C. Langway, H. Oeschger, W. Dansgaard, Eds. (Geophysical Monograph 33, American Geophysical Union, Washington, DC, 1985), pp. 90–94.
6. T. P. Guilderson, R. G. Fairbanks, J. L. Rubenstone, *Science* **263**, 663 (1994).
7. From (*4, 5*) we obtained the following: The enhancement factor for dust particles (radius > 0.4 μm) at dome C in Antarctica is 9 to 14; the enhancement factors for the elements Al, Na, and Cl are 34, 4.9, and 3.8, respectively; and the enhancement factor for dust particles in Greenland is 100.
8. C. Genthon, *Tellus* **44B**, 371 (1992).
9. S. Joussaume, *J. Geophys. Res.* **98** (D2), 2767 (1993).
10. There is no ice core data for low latitudes at sea level. However, ice cores taken from mountain glaciers show that dust contents are enhanced in the LGM layer [L. G. Thompson *et al.*, *Science* **246**, 474 (1989); L. G. Thompson *et al.*, *ibid.* **269**, 46 (1995)]. It is difficult to interpret the dust deposition rates in the high mountains because of possible changes in local meteorology during the LGM. The beauty of the polar data is that the poles are remote regions of the globe and any enhancement must be related to changes on a global scale (global change).
11. CLIMAP Project Members, *Geol. Soc. Am. Map Chart Ser.* **MC-36** (1981).
12. W. S. Broecker and G. H. Denton, *Geochim. Cosmochim. Acta* **53**, 2465 (1989).
13. V. M. Bryant Jr. and R. G. Holloway, in *Pollen Records of Late Quaternary North American Sediments*, V. M. Bryant and R. G. Holloway, Eds. (American Association of Stratigraphic Palynologists, Calgary, Ontario, 1985), pp. 39–70.
14. M. Stute, P. Schlosser, J. F. Clark, W. S. Broecker, *Science* **256**, 1000 (1992); M. Stute *et al.*, *ibid.* **269**, 379 (1995).
15. F. E. Grousset *et al.*, *Earth Planet. Sci. Lett.* **111**, 175 (1992).
16. The 2D model has four components: the photochemical module, the solar-radiative module, the infrared-radiative module, and the transport module. The model has 18 latitudes, from pole to pole. There are 40 layers, from 0 to 80 km in log pressure coodinates. Time-stepping is 1 to 4 steps per day. We usually used model times of 10 to 20 years to obtain convergence. The monthly averaged transport coefficients were computed by the method of H. Yang *et al.* [*J. Atmos. Sci.* **48**, 442 (1991)]. The details are described in R. L. Shia *et al.* [*J. Geophys. Res.* **94**, 18467 (1989)]. We adopted in the 2D model washout lifetimes computed with a 3D model by Y. J. Balkanski *et al.* [*ibid.* **98**, 20573 (1993)].
17. Our result should be compared with figure 23 in (*9*).
18. J. Jouzel *et al.*, *Quat. Res.* **31**, 135 (1989).
19. R. W. Fairbridge, *Phys. Chem. Earth* **4**, 99 (1961).
20. Recent work has shown that the total area of deserts during the LGM was about twice that in the Holocene [J. A. Chappellaz *et al.*, *Tellus* **45B**, 228 (1993); P. Friedlingstein *et al.*, *J. Geophys. Res.* **100**, 7203 (1995)].
21. G. Kukla *et al.*, *Geology* **16**, 811 (1988).
22. The saturated vapor pressure of water decreases by 34% from 30° to 25°C; thus, a change of 5°C in SST alone is not sufficient to cause a difference of a factor of 2 in the water vapor content of the atmosphere.
23. L. D. D. Harvey, *Nature* **334**, 333 (1988). We wish to speculate on the effect of atmospheric dust on the tropical "warm pool." Today a major source of moisture is the warm pool (with SSTs often >29°C) in the tropical western Pacific Ocean around Indonesia and New Guinea. If the combination of a lower ocean level (by 150 m), stronger winds, and atmospheric dust opacity were to reduce the SST of the warm pool by 10°C, this would decrease the source of moisture by half. The reduced moisture would greatly reduce the greenhouse effect caused by water vapor, thereby contributing to the cooling of the tropics.
24. The martian atmosphere is characterized by extreme aridity and dustiness, and dust plays a fundamental role in regulating the climate of Mars [J. R. Murphy *et al.*, *J. Geophys. Res.* **98**, 3197 (1993); M. Santee and D. Crisp, *ibid.*, p. 3261.

25. Supported in part by NASA grant NAGW 2204 to the California Institute of Technology and by NSC 84-2111-M-001-027GP from the National Science Council of the Republic of China. Y.L.Y. thanks the Institute of Earth Sciences and Academia Sinica for their hospitality during his sabbatical year and A. Ingersoll, L. Jaegle, C. Leovy, D. Rind, and I. Tegen for helpful discussions.

17 August 1995; accepted 1 November 1995

From Topographies to Dynamics on Multidimensional Potential Energy Surfaces of Atomic Clusters

Keith D. Ball, R. Stephen Berry,* Ralph E. Kunz,† Feng-Yin Li, Ana Proykova, David J. Wales

Multidimensional potential energy surfaces for systems larger than about 15 atoms are so complex that interpreting their topographies and the consequent dynamics requires statistical analyses of their minima and saddles. Sequences of minimum-saddle-minimum points provide a characterization of such surfaces. Two examples, Ar_{19} and $(KCl)_{32}$, illustrate how topographies govern tendencies to form glasses or "focused" structures, for example, crystals or folded proteins. Master equations relate topographies to dynamics. The balance between glass-forming and structure-seeking characters of a potential energy surface seems governed by sawtooth versus staircase topography and the associated collectivity of the growth process after nucleation.

Computational methods, particularly molecular dynamics (*1*), quenching (*2–4*), conjugate gradient minimization (*5*), and eigenvector-following (*6–11*) are now efficient enough to locate all the minima and all the important saddles on a given potential energy surface for a system consisting of as many as 10, and perhaps even 15, atoms.

However, the number of geometrically distinct minima grows at least exponentially with N, the number of particles making up the system (*3, 4, 12–15*). Consequently, cataloging all the minima for a system of about 20 or more particles is simply not productive; the added information content of most of these data is negligible. Instead, a more efficient course is a statistical approach toward characterizing the topography of the surface and, from that information, inferring the associated thermodynamics and dynamics (*16–21*). Such an analysis shows how it is possible to interpret aspects of the behavior of a system of 15 to several hundred particles, possibly many more, from a statistical sample of minima and saddles on the potential surface of the system. The method links knowledge of the forces between particles and the tendency of the system to form an amorphous structure or glass, or a "focused" structure such as a crystalline lattice, a Mackay icosahedron (*22*), or a specific folded structure such as that of a biologically active protein.

K. D. Ball, R. S. Berry, F.-Y. Li, A. Proykova, Department of Chemistry, University of Chicago, 5735 South Ellis Avenue, Chicago, IL 60637, USA.
R. E. Kunz, Institut für Theoretische Physik, Technische Universität Berlin, Hardenbergstrasse 36, D-10623 Berlin, Germany.
D. J. Wales, University Chemical Laboratories, Cambridge University, Lensfield Road, Cambridge CB2 1EW, UK.

*To whom correspondence should be addressed.
†R. E. Kunz has also published in this field under the surname Breitengraser-Kunz.

We present a general approach to characterizing topographies of given potential surfaces. The construction of these surfaces is largely separable from the analysis of their topographies; their important points of contact are the identification of regions that need to be known accurately and testing the physical plausibility of surfaces. Here, it is assumed that a single potential surface describes the motion of the atoms or molecules composing the system, and that such a surface is known. The present systems were chosen because they have been shown to be adequately described by simple interatomic potential functions. In one case, Ar_{19}, a sum of pairwise Lennard-Jones potentials suffices (*23, 24*); in the other, $(KCl)_{32}$, a sum of pairwise Born-Mayer potentials gives a satisfactory description (*25*).

The behavior of these two systems can be put into the same context as the folding of proteins and the formation of glasses. Simulations show that rare gas solids can take on amorphous structures fairly readily (*26*). In contrast, on solidification, alkali halide clusters assume rock salt structures, albeit sometimes with a few defects (*25*). It is not surprising, in view of the relative numbers of locally stable amorphous structures of the rare gas clusters, that these systems can form glasses. It is surprising, at least on a purely statistical basis, that the alkali halide clusters form rock salt lattices; the locally stable amorphous structures of $(KCl)_{32}$ outnumber the rock salt structures (*25*) by a factor of roughly 10^{12}. This ratio makes the formation of a salt crystal statistically more unlikely than the "correct" folding of a protein, the statistical improbability of which is known as Levinthal's paradox (*27*). This "paradox" is resolved on realizing that the statistical view is inappropriate for "funneling" landscapes because the global minima are not found through random searches (*28*). The salt has many more "wrong" structures than does a protein with the same number of atoms, probably because the latter is constrained to retain the integrity of the polymer chain, and the only important motions affecting the structure, apart from solvent molecules, are rotations about bonds.

Our procedure for diagnosing the topography and consequent dynamics of potential surfaces consists of the following five steps (*18, 20*). (i) Finding a representative sample of minima and saddles that link them on the potential surface and, at the same time, the eigenvalues and eigenvectors of the Hessian matrix at each of these stationary points; (ii) organizing these into triples of linked points, minimum-saddle-minimum, and ordering these triples according to the energies of their lower minima; (iii) linking the triples to each other to form sequences of minima connected by saddles; (iv) construction of a matrix of rate coefficients for passage between adjacent minima; and (v), incorporation of that matrix into a master equation and solution of that equation to obtain its eigenvalues and eigenvectors. The eigenvalues characterize rates of flow of population distributions on the potential surface, and the eigenvectors describe these flows in terms of changes in populations among the individual wells around local minima.

We found minima for both the Ar_{19} and $(KCl)_{32}$ potential surfaces by carrying out classical molecular dynamics simulations with periodic quenches (instantaneous removal of all the kinetic energy) followed by eigenvector-following to a local minimum. The saddles were found by eigenvector-following from each of the minima in the random sample. The minima linked by these saddles were then determined. For Ar_{19}, the initial sample consisted of 291 linked minima (8 unconnected minima were discarded from the initial data set) and 641 saddles that made the links. (The database was later augmented by an order of magnitude; the augmentation did not affect the conclusions.) The surface for this system probably contained at least 500,000 geometrically distinct minima, according to extrapolation from the numbers of minima for clusters of 6 to 13 atoms. The statistical sample for $(KCl)_{32}$ consisted of about 3000 minima.

The topographies of the two surfaces (Fig. 1, A and B) were clearly different. Most of the minima in our sample of the Ar_{19} surface lay on monotonic sequences of energies rising from what is generally believed to be the global minimum: the double icosahedron. The minima of the $(KCl)_{32}$ cluster fell on many monotonic sequences, which rose from various locally stable rock salt structures. The relative energies of the successive minima of the Ar_{19} cluster differed only slightly, except at the step up from the global minimum, and the barriers were mostly high, giving this surface a sawtooth topography. A previous analysis of pathways for Ar_{55} showed little correlation between barrier heights and the energies of the minima they link (*11*). The mean saddle heights of the Ar_{19} cluster increased slightly along descending sequences of minima and were generally large compared with the successive decreases in energy of those minima. The corresponding energies of successive minima on the $(KCl)_{32}$ cluster differed significantly, except in the highest reaches of the potential, and many of its saddles were low compared with

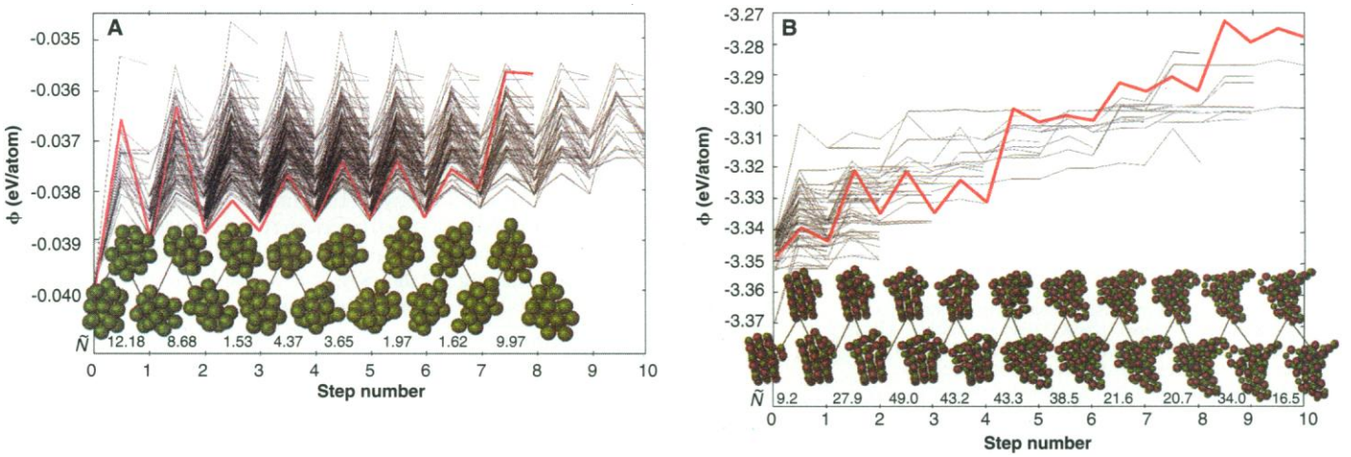

Fig. 1. (**A**) Schematic representation of the minima and saddles of the potential surface of Ar_{19}, with snapshots of the structures at a succession of minima and saddles along the emphasized sequence. (**B**) A similar representation of minima and saddles of the potential surface of $(KCl)_{32}$, with snapshots of the structures at minima and saddles along the emphasized sequence. The vertical axes are potential energies, per atom, at the configurations shown. The numbers give the cooperativity indexes for each step. Animations of these sequences are available at URL <http://rainbow.uchicago.edu/~kdb1/research/science.html> on the World Wide Web.

the larger differences of energies of successive minima. This gave the KCl surface a staircase topography. The mean saddle heights of the $(KCl)_{32}$ cluster were small between high-energy minima and grew somewhat larger as the energies of the minima decreased. However, the decreases in energy between successive minima were significantly larger than the increases in saddle height along the downward sequences.

The snapshots of the $(KCl)_{32}$ cluster (Fig. 1B) in successive minima show how nucleation and growth (*29*, *30*) of solid-like regions take the system from an amorphous structure through partially ordered forms to a final, crystal-like structure. The highest energy minima, such as that designated 9, correspond to amorphous structures. Minimum 8 corresponds to a structure with a small region, a nucleus, ordered into a rock salt–like geometry but otherwise amorphous; the energy of this structure is not very different from that of completely amorphous structures such as 9. Structures corresponding to the sequence of minima descending from 8 are successively more ordered, up to and including the final structure of the sequence. Growth of the crystalline core in this cluster did not occur predominantly by incorporation of individual ions; instead, collective motions brought clumps of ions into the growing lattice.

A measure of the cooperativity of each step along the sequence is the parameter $\tilde{N}$, which takes the value of 1 for a step associated with motion of a single particle, and of N for a step associated with cooperative motion of all N particles. $\tilde{N} = N/\gamma$, where γ is the moment ratio of displacement (*31*) defined by Stillinger and Weber (*4*). The values of $\tilde{N}$ for the succession of steps shown in the snapshots of Fig. 1A were mostly less than 5 and were well above 10 for all the steps but one shown in the snapshots of Fig. 1B. This result indicates that growth of the nucleus in the Ar cluster occurred by accommodation of one or two particles at a time, but that growth of the crystal-like nucleus in the KCl cluster occurred by collective motions.

These differences between the topographies of the two surfaces make it easy to understand why Ar_{19} is relatively difficult to bring to its (presumed) global minimum, a double icosahedron, by annealing and why $(KCl)_{32}$ is difficult to capture as a glass. In a simulation of Ar_{19} by molecular dynamics with controlled annealing (by a linear temporal decrease in temperature), cooling even as slowly as 10^9 K s^{-1} left more than half of the clusters trapped in local minima above the global minimum. A simplified Einstein model with Rice-Ramsperger-Kassel-Marcus (RRKM) (*32*) rate coefficients in a master equation for this cluster also showed similar difficulties in reaching the double icosahedron. The $(KCl)_{32}$ cluster, in contrast, found its way to a rock salt structure even if the energy was removed at 10^{12} K s^{-1}; only if the quenching is faster than about 10^{13} K s^{-1} does this system get trapped in any of the amorphous structures (*25*, *33*).

In the fourth and fifth steps of the procedure we constructed well-to-well rate coefficients and, from them, a master equation. The difference between the two kinds of clusters becomes clear in this analysis. Because the decreases in energy from one well to the next are small and the saddle heights remain roughly constant or slightly increasing down a sequence, the Ar_{19} cluster probably comes close to thermal equilibrium in each well before it passes over the next saddle. Consequently, the well-to-well rate coefficients can be estimated reliably by RRKM theory (*34*) and yield a sufficiently accurate master equation, which is linear and Markovian. In contrast, when a $(KCl)_{32}$ cluster passes downward over saddles such as those from minima 9 to 8, 5 to 4, and 2 to 1 on the heavily drawn path of Fig. 1B, the mean potential energy decreases and the mean kinetic energy increases to a value considerably higher than that in the previous well. More precisely, the mean kinetic energy in the mode associated with the saddle crossing increases momentarily. Computing the rate coefficient for passage from this newly entered well into the next well is not a simple task; the cluster may very well not be describable by a single internal vibrational temperature on the time scale of this passage. The planar projection of Fig. 1B may give a deceptive impression of simplicity. In fact, it is unlikely that the motion carrying the cluster over one saddle, for example, from 8 to 7, involves the same coordinate that carries the cluster over the next saddle, for example, from 7 to 6. However, the rate of passage over a saddle depends sensitively on the amount of energy in the mode corresponding to the reaction coordinate for that process.

The rate of passage down a sequence in a system such as $(KCl)_{32}$ involves a competition between transfer of energy into the reactive mode, especially from the mode uniquely energized by the previous saddle crossing, and transfer of energy into the sea of other modes, which act much like a thermostat. This competition not only makes the master equation more difficult to construct than in a situation satisfying a form of local thermal equilibrium, but also makes the master equation nonlinear and non-Markovian. Furthermore, such cases, in extremis, may require the introduction of specific state-to-state rate constants instead of thermalized well-to-well quantities which, in effect, incorporate averaging over modes that is fast with respect to the rates of well-to-well passages.

The analyses presented here begin to show the links from interatomic forces to topographies and a way to characterize those topographies, thence the dynamics engendered by the topography, including nucleation and growth, and finally the glass-forming or structure-seeking character. There are probably other systems that form glass structures much better than Ar_{19}, particularly clusters whose interparticle forces have very short ranges, such as clusters of C_{60} molecules (*11*, *35*); accordingly, the two examples used here cannot be called opposite extremes. Nevertheless, these examples illustrate the connection between topographies of potential surfaces and the tendencies of systems to form glasses or to seek specific structures. In this sense, Ar_{19}, with its sawtooth topography, tells us something about the atomic origins of glass formation, and $(KCl)_{32}$ tells us about crystallization by nucleation and growth and perhaps also about the folding of proteins. The funnel-like, staircase topography of the $(KCl)_{32}$ surface in Fig. 1B is similar to the kind of landscape that has been proposed recently for the potential surfaces of proteins (*28*). How far this inference can be carried will be apparent only when topographies of potential surfaces of polymers have been characterized in a manner analogous to that used here.

REFERENCES AND NOTES

1. M. P. Tildesley and D. J. Allen, *Computer Simulation of Liquids* (Oxford Univ. Press, Oxford, 1989).
2. F. H. Stillinger and T. A. Weber, *Kinam* **3**, 159 (1981).
3. ———, *Phys. Rev. A* **25**, 978 (1982); *J. Chem. Phys.* **81**, 5095 (1984); *ibid.* **83**, 4767 (1985).
4. ———, *Phys. Rev. A* **28**, 2408 (1983).
5. W. H. Press, B. P. Flannery, S. A. Teukolsky, W. T. Vetterling, *Numerical Recipes* (Cambridge Univ. Press, Cambridge, 1986).
6. J. Pancir, *Collect. Czech. Chem. Commun.* **40**, 1112 (1975).
7. C. J. Cerjan and W. H. Miller, *J. Chem. Phys.* **75**, 2800 (1981).
8. J. Simons, P. Jørgenson, H. Taylor, J. Ozment, *ibid.* **87**, 2745 (1983); A. Banerjee, N. Adams, J. Simons, *ibid.* **89**, 52 (1985).
9. J. Baker, *J. Comp. Chem.* **7**, 385 (1986).
10. D. J. Wales, *J. Chem. Phys.* **91**, 7002 (1989).
11. ———, *ibid.* **101**, 3750 (1994).
12. M. R. Hoare and J. McInnes, *J. Chem. Soc. Faraday Discuss.* **61**, 12 (1976).
13. F. H. Stillinger and T. A. Weber, *Science* **225**, 983 (1984).
14. C. J. Tsai and K. D. Jordan, *J. Phys. Chem.* **97**, 11227 (1993).
15. R. S. Berry, *ibid.* **98**, 6910 (1994).
16. G. Franke, E. R. Hilf, P. Borrmann, *J. Chem. Phys.* **98**, 3496 (1993).
17. D. J. Wales, *Mol. Phys.* **78**, 151 (1993).
18. R. S. Berry and R. E. Breitengraser-Kunz, *Phys. Rev. Lett.* **74**, 3951 (1995).
19. R. E. Breitengraser-Kunz, T. Astakhova, R. S. Berry, *Surf. Rev. Lett.*, in press.
20. R. E. Kunz and R. S. Berry, *J. Chem. Phys.* **103**, 1904 (1995).
21. J. P. K. Doye and D. J. Wales, *ibid.* **102**, 9659, 9673 (1995).
22. A. L. Mackay, *Acta Crystallogr.* **15**, 916 (1962).
23. J. A. Barker and D. Henderson, *Rev. Mod. Phys.* **48**, 587 (1976).
24. D. J. Wales, *J. Am. Chem. Soc.* **112**, 7908 (1990).
25. J. P. Rose and R. S. Berry, *J. Chem. Phys.* **98**, 3246, 3262 (1993).

26. A. Rahman, M. J. Mandell, J. P. McTague, *ibid.* **64**, 1564 (1976); F. H. Stillinger and T. A. Weber, *ibid.* **80**, 4434 (1984).
27. C. Levinthal, in *Mössbauer Spectroscopy in Biological Systems, Proceedings of a Meeting Held at Allerton House, Monticello, Illinois*, P. DeBrunner, J. Tsibris, E. Munck, Eds. (Univ. of Illinois Press, Urbana, IL, 1969), p. 22.
28. J. D. Bryngelson, J. N. Onuchic, N. D. Socci, P. G. Wolynes, *Proteins* **21**, 167 (1995); P. G. Wolynes, J. N. Onuchic, D. Thirumalai, *Science* **267**, 1619 (1995).
29. M. R. Hoare and P. Pal, *Adv. Phys.* **24**, 645 (1975).
30. B. T. Draine and E. E. Salpeter, *J. Chem. Phys.* **67**, 2230 (1977).
31. D. J. Wales, P. L. A. Popelier, A. J. Stone, *ibid.* **102**, 5556 (1995).
32. P. J. Robinson and K. A. Holbrook, *Unimolecular Reactions* (Wiley-Interscience, London, 1972).
33. H.-P. Cheng and U. Landman, *Science* **260**, 1304 (1993).
34. J. P. Rose and R. S. Berry, *J. Chem. Phys.* **96**, 517 (1992).
35. D. J. Wales, *J. Chem. Soc. Faraday Trans.* **90**, 1061 (1994).
36. We thank T. Astakhova for generating the data base of minima and saddles for the argon cluster. R.S.B. acknowledges the support of the National Science Foundation for this research. R.E.K. acknowledges the support of the Deutsche Forschungsgemeindschaft and the Sonderforschungsbereich 296. A.P. acknowledges the support of the Fulbright Scholar Program. D.J.W. gratefully acknowledges financial support from the Royal Society of London.

10 November 1995; accepted 4 January 1996

Catalytic Cleavage of the C–H and C–C Bonds of Alkanes by Surface Organometallic Chemistry: An EXAFS and IR Characterization of a Zr-H Catalyst

Judith Corker,* Frédéric Lefebvre, Christine Lécuyer, Véronique Dufaud, Françoise Quignard, Agnès Choplin, John Evans, Jean-Marie Basset*

The catalytic cleavage under hydrogen of the C–H and C–C bonds of alkanes with conventional catalysts requires high temperatures. Room-temperature hydrogenolysis of simple alkanes is possible on a well-defined and well-characterized zirconium hydride supported on silica obtained by surface organometallic chemistry. The surface structure resulting from hydrogenolysis of (≡SiO)Zr(Np)$_3$ (Np, neopentyl) was determined from the extended x-ray absorption fine structure (EXAFS) and ^{1}H and ^{29}Si solid-state nuclear magnetic resonance and infrared (IR) spectra. A mechanism for the formation of (≡SiO)$_3$Zr-H and (≡SiO)$_2$SiH$_2$ and the resulting low-temperature hydrogenolysis of alkanes is proposed. The mechanism may have implications for the catalytic formation of methane, ethane, and lower alkanes in natural gas.

The grafting of organometallic compounds onto surfaces is the basis for the rapidly developing field of surface organometallic chemistry. The reactivity of organometallic fragments with surfaces is of special relevance to the understanding of the mechanisms in heterogeneous catalysis, which are still poorly understood, and to the design of well-defined heterogeneous catalysts, which is also a challenge. The potential advantages of catalysts based on surface organometallic fragments over soluble organometallic complexes are considerable: Site isolation prevents undesirable side reactions (notably, bimolecular decomposition pathways), and the problem of catalyst separation and recovery is conveniently resolved. In some cases, it has been shown that surface organometallic fragments show substantially enhanced reactivity and selectivity compared to analogous molecular complexes or classical heterogeneous catalysts. We report here how the design of a well-characterized zirconium hydride supported on silica can lead to a solid with remarkable catalytic activity for alkane activation.

The catalytic cleavage of the C–H and C–C bonds of higher alkanes (paraffins) is also a subject of considerable importance. Paraffins are inert materials: Their transformation to lower alkanes (by hydrogenolysis) or to fuels (by dehydrocyclization) usually requires heterogeneous catalysts working at rather high temperatures (typically 500°C). If such reactions could be carried out at a much lower temperature, it would be of great economical advantage. Similar reactions may also play a role in the formation of natural gas (*1*); it has recently been proposed that ethane and methane may be formed catalytically rather than by thermal decomposition of sedimentary organic matter (*1*). This hypothesis could alter the way in which we view the generation and distribution of oil and gas in the Earth.

We have discovered that it is possible to carry out the catalytic hydrogenolysis of several simple alkanes (for example, propane, butanes, and pentanes, with the exception of ethane) at mild temperatures by means of a catalyst consisting of a zirconium hydride supported on silica obtained by surface organometallic chemistry (*2*–*6*). For example, neopentane (Np-H) was converted into isobutane and methane by the catalyst Zr-H/SiO_2 in the presence of H_2 (1 atm) at 25°C after several hours. If long reaction times (several days) were used, the final products were exclusively methane and ethane (an alkane that is not cleaved by the catalyst under hydrogen). Classical heterogeneous or even homogeneous catalysts and enzymes normally do not achieve under hydrogen such facile cleavage of the C–C bonds of simple alkanes into ethane and methanes (*5*). We report here the structure of the catalyst and its precursor at an atomic and molecular level. Hereby, we wish to show how this activity can be achieved.

Table 1. The Zr K-edge EXAFS-derived structural parameters for the grafted Zr complexes on silica dehydroxylated at 500°C. For Zr K-edge spectra, AFAC = 0.89* and VPI = −2.0 eV†; values of the photoelectron energy at zero wave vector (E_0) for samples (≡Si–O)ZrNp$_3$ and (≡S–O)$_3$ZrH were 13.5 and 20.7 eV, respectively. The Debye-Waller factor is given as $2\sigma^2$, where σ is the root-mean-square internuclear separation. The values given in parentheses represent the statistical errors generated in EXCURVE; for true error estimation, see (*6*).

Shell	Coordination number	Distance R (Å)	$2\sigma^2$ (Å^2)	R factor (%)
		(≡Si–O)ZrNp$_3$		
O	1.1(1)	1.956(3)	0.0066(8)	29.7
C	3.2(1)	2.219(4)	0.0163(9)	
C	2.8(3)	3.42(1)	0.026(3)	
		(≡Si–O)$_3$ZrH		
O	3.1(1)	1.945(3)	0.0170(5)	27.4
O	1.1(2)	2.61(1)	0.018(3)	

*AFAC, a nondimensional factor describing the effects of multiple excitations resulting in the reduction of EXAFS amplitude, taken to be independent of the environment around the absorbing atom. †VPI, constant imaginary potential describing the lifetime of the photoelectron, describes effects of inelastic scattering in curved wave theory.

J. Corker and J. Evans, Department of Chemistry, University of Southampton, Southampton SO9 5NH, UK.
F. Lefebvre, C. Lécuyer, V. Dufaud, J.-M. Basset, Laboratoire de Chimie Organométallique de Surface, Unité Mixte de Recherche 9986, Centre National de Recherche Scientifique (CNRS)–Ecole Supérieure de Chimie, Physique, et Electronique de Lyon (CPE-Lyon), 69616 Villeurbanne Cedex, France.
F. Quignard and A. Choplin, Institut de Recherches sur la Catalyse, CNRS, 69626 Villeurbanne Cedex, France.
*To whom correspondence should be addressed.